Surface segregation trends in transition metal alloys

J. H. Los,[1,2] C. Mottet,[1] and G. Tréglia[1]

[1]*Centre Interdisciplinaire de Nanoscience de Marseille (CINaM), UMR 7325 CNRS-AMU, Campus de Luminy, case 913, 13288 Marseille, Cedex 9, France*

[2]*Institute of Physical Chemistry and Center for Computational Science, Johannes Gutenberg University Mainz, Staudinger Weg 9, D-55128 Mainz, Germany*

(Received 13 February 2013; revised manuscript received 25 July 2013; published 11 October 2013)

In this work, we revisit the problem of predicting the surface segregation trends in binary transition metal alloys from the knowledge of the basic features of the pure component d-band electronic structure within tight-binding approximation. In contrast to previous trend studies, the present one includes, within the fourth-moment approximation (FMA) of the tight-binding scheme, both the difference in the average band energies (diagonal disorder) and the difference in the band widths (off-diagonal disorder) of the two components. We show that treating on the same footing these two effects is essential for a correct prediction of surface segregation. The presented study, giving a natural link between the electronic structure and mixing/segregation properties, is particularly interesting and useful in the context of the possibility of building efficient new energy models based on FMA for use in large (time) scale atomistic simulations.

DOI: 10.1103/PhysRevB.88.165408 PACS number(s): 71.20.Be, 61.66.Dk, 68.35.bd, 45.70.Mg

I. INTRODUCTION

Surface segregation in transition metal alloys is a recurrent problem which has given rise to intensive investigations both theoretically[1–7] and experimentally[8–10] in the last twenties. This phenomenon finds a renewed interest with the bimetallic nanoparticles, also called nanoalloys, where the surface plays an important role as it can represent almost as many sites as the core of the cluster. Since the first studies mainly devoted to their catalytic properties,[11] these nanoalloys have also shown many other potential applications, amongst others in magnetic information storage or in plasmonic.[12] Nanoalloys present new technological and fundamental problems, which are now revisited through modern tools and adaptation of the classical tools, both from an experimental and a theoretical point of view, and in the first place devoted to surface analysis.[13]

A first aim of the present work is to derive and understand the trends in surface segregation properties of binary transition metal alloys from the knowledge of the basic features of the pure element electronic structure, in particular, the difference in the average d-band energy, called diagonal disorder, and in the d-band widths, that is off-diagonal disorder, of the two species involved. Obviously, such an understanding is extremely useful when it comes to invent new materials with desired properties.

Previous works on metallic surfaces[6,14] have been devoted to predict the nature of the segregation species or described the main driving forces of surface segregation phenomena.[15,16] Among all the theoretical approaches that exist to model the cohesion in transition metals and their alloys, *ab initio* density functional theory (DFT) methods are certainly the most accurate and can also give some insights for new materials design as demonstrated by Johannesson and co-workers[17] who used DFT calculation coupled with an evolutionary algorithm to search efficiently for the most stable alloys among all the binary alloys. Nevertheless, such approach is still very computer time consuming. On the contrary, semiempirical models have been developed, based on tight binding within the second-moment approximation (SMA), which enable the study of large, complex structures of alloys and notably the statistical mechanics of their chemical configurations using (semi)grand canonical simulation techniques.[18,19] However, such models are sometimes too simple to satisfy a desired level of accuracy. In particular, the SMA model only includes off-diagonal disorder, whereas it has been shown[20] that the difference in the atomic levels (diagonal disorder) is of crucial importance for the ordering/demixing tendency in transition metal alloys. The impact of diagonal disorder has therefore been studied within yet another approach, based on the so-called tight-binding Ising model (TBIM),[21–23] but this approach does not take into account nondiagonal disorder.

It is to solve this contradiction that we have used a tight-binding approach based of the fourth-moment approximation (FMA) in order to quantify the effects of both diagonal and off-diagonal disorder and give exhaustive ordering trends in bulk alloys.[24] Indeed, the mentioned study based on the TBIM, including only diagonal disorder, predicts a demixing tendency for low band filling (early transition metals) or high band filling (late transition metals), and ordering in between.[21,22] This trends is globally correct but there are exceptions notably in the late transition metals, such as CuAu or CoPt, which display a clear ordering tendency. We have shown that these cases are solved (or partially solved in the case of CoPt) by including nondiagonal disorder.[24] Concerning CoPt, we note that a possible effect from magnetism,[27] due to Co, was not considered in our study. Here, we extend our previous work by studying the effects of both diagonal and off-diagonal disorder on the surface segregation tendency along the transition metals series. For surface segregation, it was found within the TBIM that surface segregation trends are rather strongly related to the difference in surface energies of the two pure elements, at least when the other driving forces (alloying effect and size mismatch effects) are not so important, the element with the lowest surface energy segregating to the surface in many cases. These trends are compatible with most of the experimental observations when available,[8,14] albeit again with exceptions, possibly (and partly) related to the neglection of nondiagonal

disorder. All these results have shown that, complementary to the predictions of DFT calculations,[3,5,6] the identification of the driving forces behind ordering/demixing and segregation trends from more simple models and ingredients, as initiated by the TBIM studies, is an interesting topic providing useful results. They also prompt to an extension by including nondiagonal disorder, as given here.

From the point of view of surface alloys and nanoalloys modeling, the FMA is a natural and ideal starting point for constructing computationally efficient total energy models for use in large scale, atomistic simulations. FMA goes beyond the well-known and widely used models based on or equivalent to the SMA,[25,26] such as embedded atom models[28–32] or bond order potentials,[33–36] and has already been successfully parameterized and used for carbon-nickel systems.[37,38] By construction, the computational effort for FMA scales linearly with the system size, like SMA. In practice, FMA is not much slower (typically less than an order of magnitude) than SMA based models and therefore allows for large scale atomistic simulation well beyond the reach of *ab initio* methods (within DFT) or even standard tight-binding. Improvements of the SMA models in this direction, known as analytical bond order potentials,[39–42] have been proposed earlier, but these models do not give an explicit link between the total energy expression and details of the electronic structure. Instead, the FMA model includes a description of the electronic structure, which is essential for the present work.

In the present trend study, we will use the FMA model with canonical rules for the tight-binding parameters, i.e., omitting the parameter fine-tuning required for an optimally accurate description of a particular pair of elements. It may be clear that regarding accuracy such a canonical FMA model cannot compete with calculations at an *ab initio* level within density functional theory (DFT). Also, as in our previous study, our model does not include spin polarization, which could be only significant for the few magnetic transition metals (Fe, Co, Ni) for which a lowering of the segregation energy has been predicted.[43]

The paper is organized as follows: after this introduction, the theory description is detailed in Sec. II, bulk order/demixing trends are presented in Sec. III and surface segregation trends in Sec. IV. A brief summary and conclusions are given in Sec. V.

II. THEORY

A. Tight-binding model for transition metals and their alloys

Within a tight-binding description, the wave function, describing the quantum state of the system, is expressed as a linear combination of localized atomic orbitals. Eventually, this leads to a Hamiltonian matrix H_{TB}, which for a crystal has an eigenvalue spectrum consisting of an energy band or possibly bands and gap(s). Roughly speaking, the diagonal blocks of H_{TB} determine the average band energy/energies [that is, its/their position(s) on the energy axis], whereas the off-diagonal blocks, which describe the probabilities for electron hopping between atoms, determine the width(s) of the band(s).

The band structure according to H_{TB} together with the filling of it up to the Fermi level E_F, depending on the number of available valence electrons, determine the electronic, or band energy E_{band} of the system. The total energy of a tight-binding model is obtained by adding to this a repulsive contribution, which usually is empirical and consists of a sum of repulsive pair interactions.

For transition metals, it is well known that the dominant and decisive contribution to the density of states comes from the d-band, with band fillings running from 0 to 10 for each of the three transition metal series. Hence we may describe a transition metal within a pure d-band basis set, $|\lambda\rangle(\lambda = 1,5)$, by the Hamiltonian

$$H_{\mathrm{TB}} = \sum_{i,\lambda} |i\lambda\rangle \varepsilon^{\lambda} \langle i\lambda| + \sum_{\substack{i,\lambda \\ j\neq i,\mu}} |i\lambda\rangle \beta_{ij}^{\lambda\mu} \langle j\mu|, \qquad (1)$$

where the sums over i and j run over all N atoms, the diagonal parameter ε^{λ} is the isolated atom electronic energy level for the orbital $|\lambda\rangle$, and the off-diagonal parameters $\beta_{ij}^{\lambda\mu}$ are the hopping integral matrix elements. For transition metals, the crystal field splitting between the atomic ε^{λ} levels, i.e., the difference between t_{2g} and e_g levels, is much smaller than the d-band width (a few hundred of meV compared to a few eV[44]). Therefore we will neglect this splitting and take $\varepsilon^{\lambda} = \varepsilon$ for $\lambda = 1,\ldots,5$. Each of the hopping probabilities $\beta_{ij}^{\lambda\mu}$ are standardly described by the Slater-Koster two-center integrals[45] and consists of a sum of terms, where each term can be factorized into a bond orientation dependent part, which is universal (i.e., species independent), and a purely bond distance dependent potential, which is either $dd\sigma(r)$, $dd\pi(r)$, or $dd\delta(r)$, corresponding to the three possible hybridization channels. In general, these potentials have a finite cutoff, which may be chosen such that only nearest neighbors yields nonzero hopping integrals. We have adopted this approximation in the present work. For our lattice calculations, the r dependence of these potentials, often taken as simple exponential functions, is irrelevant and we only need their equilibrium values, $dd\alpha_{\mathrm{eq}} \equiv dd\alpha(r_{\mathrm{eq}})(\alpha = \sigma,\pi,\delta)$, where r_{eq} is the equilibrium nearest-neighbor distance. Furthermore, adopting the well-established canonical rules $dd\pi \simeq -dd\sigma/2$ and $dd\delta \simeq 0$,[44] the d-band width for the fcc lattice can be analytically derived to be equal to $W = -6dd\sigma_{\mathrm{eq}} + 4dd\pi_{\mathrm{eq}} + 2dd\delta_{\mathrm{eq}} \simeq -8dd\sigma_{\mathrm{eq}}$.[20] Finally, since we assume an orthogonal TB model in this work, the overlap matrix is the identity matrix not containing additional parameters.

Of the two parameters left in the above description, i.e., ε and W, ε is not really a free parameter as it has to be compensated by an equal energy shift to ensure that E_{band} vanishes in the isolated atoms limit. Hence we can conclude that in a first reasonable approximation, the d-band energy of a transition metal on a fcc lattice is determined by merely one parameter, namely the off-diagonal parameter or bandwidth $W = -8dd\sigma_{\mathrm{eq}}$.

If we now move to binary alloys, the Hamiltonian extends to

$$H_{\mathrm{TB}}(\{p_{ia}\}) = \sum_{a,i,\lambda} p_{ia} |i\lambda\rangle \varepsilon_a \langle i\lambda| + \sum_{\substack{a,i,\lambda \\ b,j\neq i,\mu}} p_{ia} p_{jb} |i\lambda\rangle \beta_{ij,ab}^{\lambda\mu} \langle j\mu|, \qquad (2)$$

where p_{ia} are site occupation numbers, with $p_{ia} = 1$ if site i is occupied by an atom of type a ($a = A,B$) and $p_{ia} = 0$ otherwise, and where we assumed ε_a to be independent on the d orbital λ as before. While the bond orientation dependent part of $\beta_{ij,ab}^{\lambda\mu}$ is independent of the chemical identities of the atoms i and j, the parameterization of the distance dependent part can be reasonably restricted by using the so-called Shiba rule $dd\alpha_{AB} = \sqrt{dd\alpha_{AA}dd\alpha_{BB}}(\alpha = \sigma,\pi,\delta)$. Adopting this rule and defining $W_a = -8dd\sigma_{aa,\mathrm{eq}}(a = A,B)$, the band energy of any binary alloy from the three transition metal series on an fcc lattice is, apart from its composition x_B (with $x_B = 1 - x_A$ in mole fraction) and corresponding band filling $N_e = x_A N_{e,A} + x_B N_{e,B}$ [with $N_{e,a}(a = A,B)$ the number of d electrons of each metal], determined by merely three parameters, which are appropriately chosen as the *diagonal disorder parameter* $\delta_d \equiv \varepsilon_A - \varepsilon_B$, the *off-diagonal disorder parameter* $\delta_{nd} = W_A - W_B$, and the average bandwidth parameter $W_{\mathrm{av}} = (W_A + W_B)/2$. At this point, it is important to notice that each of these parameters is based on pure element parameters. This means that the major trends in the mixing and surface segregation properties, as presented in Secs. III and IV, are basically determined by pure element electronic properties. Obviously, also the band filling N_e is based on pure element properties. It should be noticed, however, that there is an intrinsic correlation between the parameters due to the constraint of local charge neutrality, a property of transition metal alloys recently confirmed by DFT calculations,[46] and which even holds at surfaces.

As has been shown in our previous work on bulk ordering properties,[24] the impact of the average band parameter W_{av} is, although not negligible, relatively small. Therefore, to keep the present work concise, we will mainly restrict ourselves to the role of the *diagonal* and *off-diagonal disorder* parameters, δ_d and δ_{nd}, taking W_{av} equal to a representative, average value for the transition metals.

Further refinements, that can be obtained by relaxing the above mentioned approximations, will not change the major trends, but lead to relatively small quantitative modifications. In general, this also holds for the impact of the repulsive part of the TB model. For transition metals, the repulsive interaction at normal conditions is relatively small as compared to the band energy (namely, about twenty percents at the equilibrium distance[20]). Moreover, the ordering systematics experimentally evidenced along each transition metal series, i.e., as a function of the d-band filling, implies that the band term is the leading one for such behaviours at least for systems that do not present a large size mismatch. Larger quantitative effects for the segregation can be expected, however, for two elements with rather different sizes, in particular, when one would allow the structure to relax. In this work, we will not consider this so-called size effect but focus on the major effect coming from the band part of the total energy, which is the dominant driving force in most cases. However, for a more complete prediction of the segregation behavior for a particular alloy, one could, in principle, add the size effect as estimated from elasticity theory, as is done in Ref. 14, involving the bulk and shear moduli for the issued alloy. Another possibility is to parameterize an FMA potential, including the repulsive interaction, in order to simulate explicitly the atomic relaxations using quenched molecular dynamics. The presented study is based on electronic energy differences of rigid lattice configurations, omitting the repulsive interactions.

It should be realized that the pure component parameters ϵ_a and W_a are correlated and basically known for all three transition metal series from the work in Ref. 44. This correlation is clearly demonstrated by a plot of W_a versus ϵ_a for the three transition metal series (see Fig. 1 in Ref. 24). Deriving δ_d and δ_{nd} from this work yields values in the ranges $0 < \delta_d < 10$ eV and $-10 < \delta_{nd} < 10$ eV, taking δ_d positive without loss of generality. However, for many transition metal alloys, among which those of our particular interest, δ_d and $|\delta_{nd}|$ are not larger than 4 eV. Therefore the parameter values for the calculations presented later on have been chosen within these more limited ranges. The average band parameter W_{av} was taken equal to 6 eV in all cases.

B. Fourth-moment approximation (FMA)

The total band energy E_{band} can be decomposed into atomic band energies $E_{\mathrm{band},i}$ as

$$E_{\mathrm{band}} = \sum_{i=1}^{N} E_{\mathrm{band},i} = \sum_{i=1}^{N} 2\int_{-\infty}^{E_F} (E - \epsilon_i) n_i(E) dE, \quad (3)$$

where the prefactor 2 accounts for the two spin states in the paramagnetic state, E_F is the Fermi energy, ϵ_i is the average d-orbital energy per electron in an isolated atom i, and $n_i(E)$ is the local density of states (LDOS) at the position of atom i. Via the Green's function formalism, the d-band LDOS can be written as $n_i(E) = -(5/\pi)\lim_{\epsilon\to 0^+} \mathrm{Im}[1/(zI - H_{\mathrm{TB}})]$, where $z = E + i\epsilon$, which can be worked out to the continued fraction expansion:

$$n_i(E) = -\frac{5}{\pi}\lim_{\epsilon\to 0^+} \mathrm{Im}\left(\cfrac{1}{z - a_{i,1} - \cfrac{b_{i,1}^2}{z - a_{i,2} - \cfrac{b_{i,2}^2}{z - a_{i,3} - b_{i,3}^2/\ddots}}}\right), \quad (4)$$

where $a_{i,n}$ and $b_{i,n}$ are the continued fraction coefficients, which can be computed from the recursion method.[47]

The fourth-moment approximation consists of taking $a_{i,n} = a_{i,2}$ and $b_{i,n} = b_{i,2}$ for all $n > 2$. This terminates the tail of the continued fraction expansion, leading to an analytic expression for $n_i(E)$[38] with the important property that both $n_i(E)$ and $En_i(E)$ are analytically integrable,[38,48] allowing for fast and accurate computation.

In the FMA, the LDOS is thus based on the four computed coefficients $a_{i,n}$ and $b_{i,n}$ for $n = 1,2$, which ensures to get the first four exact moments $\mu_{i,n}(i = 1,4)$:

$$\mu_{i,n} = \frac{1}{5}\int_{-\infty}^{\infty} E^n n_i(E) dE = \frac{1}{5}\sum_{\lambda}\langle i\lambda|H_{\mathrm{TB}}^n|i\lambda\rangle \quad (5)$$

for $n = 0$ to 4. Note that $\mu_{i,0} = 1$ by normalization.

It appears from this formulation that the exact calculation of the nth moment $\mu_{i,n}$ involves all n-hopping closed paths starting from atom i. This means that SMA, which only counts two-hopping paths, only feels off-diagonal disorder, whereas one needs to go up to the fourth moment to be also sensitive to diagonal disorder. Indeed, the fourth-moment pathway $i \to i \to j \to j \to i$, where j is a neighbor of i, involves both

the diagonal matrix element for specie i and that for specie j, represented by the parts $i \to i$ and $j \to j$, respectively. Within the SMA, the chemical nature of the neighbor atom j is only included via the off-diagonal term $i \to j$ appearing in second-moment pathways $i \to j \to i$.

C. Tight-binding Ising model: effective pair interactions and surface potential

As a starting point for deriving and identifying quantities that dominate the mixing and surface segregation properties, we use the so-called cluster expansion in which the energy is expanded as a systematic sum of n-body terms ($n = 0,1,2,3,\ldots$). For a mixture with an arbitrary number of components, the cluster expansion reads

$$E = NE_0 + \sum_i \sum_a p_{ia} h_{ia} + \sum_{\langle i,j \rangle} \sum_{a,b} p_{ia} p_{jb} V_{ij,ab} + \cdots, \tag{6}$$

where the sums over i and $\langle i,j \rangle$ run over all atomic sites and pairs of sites, respectively, the sums over a and b run over the atomic species, and where p_{ia} has been defined before. In expression (6), E_0, h_{ia}, and $V_{ij,ab}$ are a constant, site potentials and pair potentials, respectively. Although it is well known that a reasonable description of the cohesive energy of transition metals requires to go beyond pair terms due to many-body effects, it has been previously shown from a perturbation treatment that the configuration dependent part of this energy is well described by the cluster expansion truncated beyond pair terms, which then turns into a generalized Ising model, known as TBIM.[21–23] Hence, we will continue with this truncated expansion, the TBIM.

In principle, h_{ia} and $V_{ij,ab}$ depend on the site i and pair of sites ij, respectively, as well as on their respective occupations by a and ab. However, in a bulk lattice model with one atom in the primitive unit cell, where all sites are geometrically equivalent, we can simplify the TBIM to

$$E = NE_0 + \sum_a N_a h_a + \sum_l \sum_{\langle ab \rangle} N_{ab}^{(l)} V_{ab}^{(l)}, \tag{7}$$

where N_a is the number of atoms of type a, N_{ab}^l is the number of lth neighbor pairs of type ab, h_a is a specie dependent site potential and $V_{ab}^{(1)}$, $V_{ab}^{(2)}$, etc., are pair interactions between first, second, etc. neighbors. In this work, we will retain only the pair interactions between nearest neighbors, as they represent by far the dominant contribution in the fcc crystalline structure.[22] In the following, we will therefore omit the superscript (1), writing $N_{ab}(=N_{ab}^{(1)})$ and $V_{ab}(=V_{ab}^{(1)})$ for convenience. Also, we will consider a binary alloy from now on. Then, for a bulk phase, the quantities $N_a (a = A,B)$ and $N_{ab} (ab = AA,BB,AB)$ are not independent but satisfy the exact relations:

$$N_{AA} = \tfrac{1}{2}(ZN_A - N_{AB}) \quad \text{and} \quad N_{BB} = \tfrac{1}{2}(ZN_B - N_{AB}), \tag{8}$$

where Z is the number of nearest neighbors, with $Z = 12$ for an fcc crystal. Substitution of these relations into Eq. (7) leads to

$$E = \sum_a N_a E_a - N_{AB} V, \tag{9}$$

where $E_a = E_0 + h_a + \frac{Z}{2} V_{aa}$ and V is the (nearest neighbor) effective pair potential defined as

$$V = \tfrac{1}{2} V_{AA} + \tfrac{1}{2} V_{BB} - V_{AB}. \tag{10}$$

This effective pair interaction is directly related to the excess energy per AB bond, $V_E = -V$, used in the field of thermodynamics of mixtures.

Equation (9) implies that for a fixed composition $x_B = N_B/N$ the total energy for any configuration depends only on the number of nearest neighbor pairs of type AB, N_{AB}, as the terms $N_a h_a (a = A,B)$ are constant. Hence, within this approximation up to nearest-neighbor-pair interactions, the mixing behavior is governed by the sign of V. Positive and negative V correspond to a tendency to mixing and demixing, respectively.

For studying surface segregation properties, we will use slab geometries of the fcc lattice with the two surfaces chosen perpendicular to the z direction and periodic boundary conditions applied in the x and y directions. Clearly, now not all sites are geometrically equivalent, so that, staying within the TBIM, in general Eq. (7) will not be a good approximation anymore. The simplest extension to improve the expansion (7) is to distinguish between two types of site potentials, one for bulk sites h_a and one for surface sites h_a^s on the basis of their nearest neighbor coordination. In that case, Eq. (7) generalizes to

$$E \simeq NE_0 + \sum_a N_a h_a + \sum_{\langle ab \rangle} N_{ab} V_{ab} + \sum_a N_a^s \left(h_a^s - h_a\right), \tag{11}$$

where N_a^s is the number of atoms of type a at the surface and h_a^s the site potential at the surface for an atom of type a. For a slab, the relations (8) have to be replaced by

$$\begin{aligned} N_{AA} &= \frac{1}{2}(ZN_A - N_{AB}) - \frac{Z'}{2} N_A^s \quad \text{and} \\ N_{BB} &= \frac{1}{2}(ZN_B - N_{AB}) - \frac{Z'}{2} N_B^s, \end{aligned} \tag{12}$$

respectively, where Z' is the number of broken bonds of an atom at the surface, assuming that all surface sites are equivalent, which is the case for the high symmetry (001) and (111) surfaces of the fcc lattice. Substitution of Eq. (12) into (11) and some rearrangements lead to

$$E \simeq \sum_a N_a E_a + \frac{1}{2} N^s \Sigma^s - N_{AB} V + \frac{1}{2} \Delta N^s \Delta h^s, \tag{13}$$

where we defined $N^s = N_A^s + N_B^s$, $\Delta N^s = N_A^s - N_B^s$, $\Sigma^s = h_A^s + h_B^s - h_A - h_B - \frac{Z'}{2}(V_{AA} + V_{BB})$ and

$$\Delta h^s = h_A^s - h_B^s - h_A + h_B - \frac{Z'}{2}(V_{AA} - V_{BB}), \tag{14}$$

which we will call the effective surface potential hereafter. Looking at it naively, within the TBIM this surface potential is nothing else than the difference in the surface energy for a pure A slab and that for a pure B slab, including

a surface site contribution, $(h^s_A - h_A) - (h^s_B - h_B)$, and a missing pair terms (or broken bonds) contribution. Indeed, applying the TBIM to pure slabs yields surface energies equal to $E^s_a = h^s_a - h_a - Z'V_{aa}/2 (a = A, B)$. However, although the TBIM gives good approximations of the energy difference between configurations with the same composition, there is no reason to assume that this truncated expansion (TBIM) gives reliable energy differences between structures with different compositions. Nevertheless, it can be derived that,[23] when off-diagonal disorder is neglected and appropriate band fillings are used for the pure slabs (see Sec. IV), this correspondence between the effective surface potential and the difference in the pure component surface energies should hold fairly well, as was shown explicitly for the compositions $x_B = 0.25, 0.5, 0.75$.[23] This is the reason why the segregation tendency is often determined by computing this difference in the surface energies. However, it remains to be seen to what extent this approach remains valid/accurate when off-diagonal disorder is taken into account and for dilute mixtures. In Sec. III, we will show that in particular for dilute mixtures strong deviations from this often assumed relation between segregation tendency and pure component surface energy difference can be expected.

For slab configurations with fixed composition, only the last two terms on the right-hand side of Eq. (13) vary, depending on the values of N_{AB} and ΔN^s for a particular configuration. Thus, comparing energies for slab configurations with equal N_A, N_B, and N_{AB}, the surface segregation behavior is governed by the sign of Δh^s, with a tendency for A/B-terminated surfaces for negative/positive Δh^s.

III. BULK ORDER/DISORDER TRENDS

According to Eq. (9), the effective pair interactions can be conveniently calculated from the formation energy of a system 1 from another system 2 with equal N_A and N_B but different N_{AB} from

$$V = -\frac{E_1 - E_2}{N_{AB,1} - N_{AB,2}}, \tag{15}$$

where the subscripts 1 and 2 label the two systems with electronic energies E_1 and E_2, computed using the FMA model in our case. (Note that $E_1 - E_2$ could be calculated from a model at any level accuracy.) Furthermore, we will use the fact that charge transfer is negligible in transition metal alloys.[46] This implies that the integrations over $\varepsilon_i n_i(E)$ in Eq. (3) cancel out in the calculation of $E_1 - E_2$, so that

$$E_1 - E_2 = 2\sum_{i=1}^{N}\left(\int_{\infty}^{E_{F,1}} E n_{1,i}(E)dE - \int_{\infty}^{E_{F,2}} E n_{2,i}(E)dE\right). \tag{16}$$

It should be reminded, however, that application of Eq. (16) to a real transition metal requires a self-consistent value for δ_d, i.e., a value that yields local neutrality. Note that as long as we do not specify a particular binary by the individual band fillings of both components but only use the average band filling (N_e) (as is sufficient for our model), this self-consistency constraint does not enter our calculations. However, when we want to calculate the effective pair interactions for a given, real transition metal alloy, we should either perform a self-consistent calculation leading to a self-consistent value of δ_d or, alternatively, use a self-consistent value available in literature.[49]

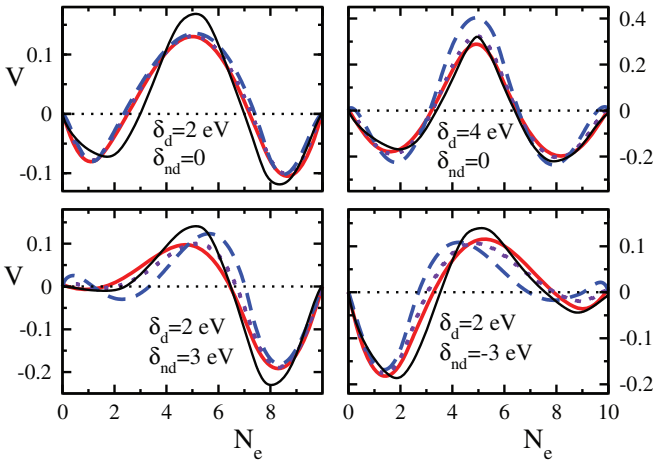

FIG. 1. (Color online) The effective pair potential V (in eV) as a function of the d-band filling N_e, calculated from the formation energy of the $L1_0$ phase (solid red line), the formation of two realizations of disordered phases (indigo dotted lines), and the formation energy of a bulk slab configuration (see text, blue dashed line). The thin, black solid line are the results obtained from calculations based on 22 exact moments.

We have calculated V from the formation energy of a mixed system 1 from a system 2, where the latter is taken as the weighted sum of the pure phases with total density of states equal to $\sum_i^N n_{2,i} = N_A n_A + N_B n_B$, with n_A and n_B the local densities of states for the pure phases. Results for $x_B = 0.5$ are shown in Fig. 1 for different choices of the mixed system 1, including the ordered $L1_0$ phase, two disordered phases and a phase consisting of periodically repeated slabs of four layers A alternated with four layers B. In the $L1_0$ phase, the two atoms species are arranged in alternating layers perpendicular to one of the axis of conventional cubic lattice for the fcc structure. Let us first consider what happens when off-diagonal disorder is neglected. Looking at the case $(\delta_d, \delta_{nd}) = (2,0)$ eV in the left top panel, we find a tendency to demix for low and high d-band filling and to mix for intermediate band filling, in agreement with the prediction derived from the generalized perturbation method.[21,22] The results are practically independent of the choice of system 1, which confirms that the effective pair interaction, derived from the cluster expansion neglecting all terms beyond nearest neighbors, is indeed the appropriate quantity and dominant term for the mixing behavior. Note that the observed difference in Fig. 1 could be translated in terms of higher order terms of the cluster expansion but apparently these terms are relatively small. The right top panel for $(\delta_d, \delta_{nd}) = (4,0)$ eV shows that $|V|$ increases with increasing δ_d, as expected. If one now introduces off-diagonal disorder, one can see in the lower panels that its effect is to strongly decrease/enhance the demixing tendency for low/high band filling when δ_{nd} is positive and vice versa when δ_{nd} is negative.

One can then wonder to what extent these systematic trends hold when a higher number of exact moments is used to calculate the density of states. In order to check that the FMA development is sufficient (and crucial when putting it against

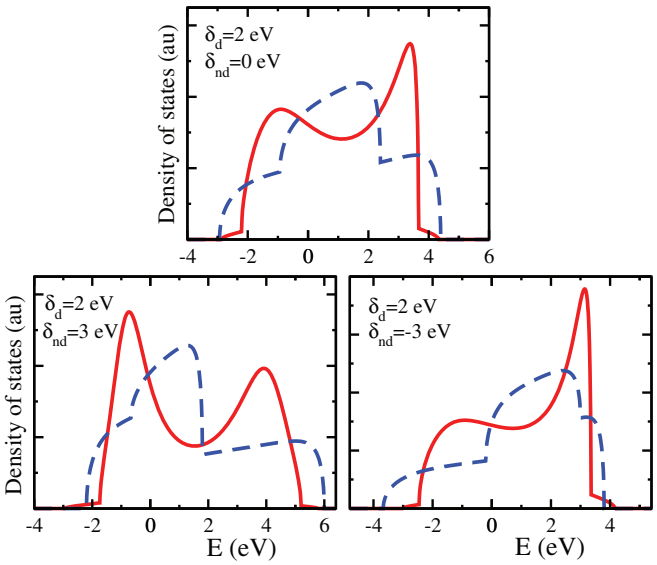

FIG. 2. (Color online) Total density of states for the $L1_0$ ordered phase (solid, red line) and weighed sum of the densities of states for the pure phases, $n(E) = 1/2[n_A(E) + n_B(E)]$ (dashed, blue line).

the SMA) to capture the essential physics of the ordering phenomena, we have calculated these effective ordering pair interactions using 22 exact moments yielding a much more precise description of the electronic structure. As can be seen in Fig. 1, the agreement between calculations with 4 and 22 exact moments fully justifies the use of FMA.

The observed behavior in Fig. 1 can be understood by looking at and comparing the densities of states of system 1 and system 2, shown in Fig. 2 for the case that system 1 is the $L1_0$ phase. In view of Eqs. (15) and (16), V is determined by the integral over $E\Delta n = E(n_{AB} - n_A/2 - n_B/2)$, where n_{AB} is the total density of the mixed ($L1_0$) phase. Looking first at the case $\delta_{nd} = 0$ in the top panel, we observe that n_{AB} (solid, red line) is narrower than $n_A/2 + n_B/2$ (dashed blue line), leading to the situation that the density of bonding states at the lower band edge is larger for the demixed state (dashed, blue line) than that for the mixed state. Hence, for small average band filling N_e, the demixed state is energetically favorable, which is then reflected in the negative sign of V in Fig. 1 for this case at small N_e. Subsequently, for increasing band filling, we enter in a region where $\Delta n(E)$ changes sign, as can be deduced from Fig. 2 by looking at the difference between the two curves. At a certain point, this then leads to a change of sign of the integrated quantity V, etc. So, in essence, the behavior of the sign of V is related to the enhanced narrowness of n_{AB} as compared to $n_A/2 + n_B/2$, which in turn can be fully explained by what is analytically known of the eigenvalue spectrum of a real symmetric matrix (H_{TB}) with diagonal disorder.[20] However, when nondiagonal disorder is added and, in particular, when $\delta_{nd} > \delta_d$, this analytical analysis breaks down partially. But what happens in such cases according to our calculations is shown in the bottom panels of Fig. 2. For the case that W_A is larger than W_B, i.e., for positive $\delta_{nd} = 3$ eV, n_{AB} shows an increased density at low energy due the contribution from the narrower but larger B band density at these low energies (shifted down by $\delta_d = 2$ eV with respect to the A band). Due to the hybridization in the mixed phase, this pushes the lowest energies of n_{AB} to values even lower than those at the lower band edge of $n_A(E)/2 + n_B(E)/2$, which in turn leads to a very tiny region, i.e., only for very small N_e, in the corresponding panel in Fig. 1 where V is positive. For the $L1_0$ this is hard to see in Fig. 1, as it concerns only very small N_e, but for the bulk slab configuration it is much more pronounced. In both case, the underlying mechanism is the same. This discussion can be extrapolated to explain the behavior of V for negative δ_{nd} as well, looking at the right bottom panel of Fig. 2.

As a conclusion for bulk materials, one can state that the off-diagonal disorder strongly modifies order-disorder maps in the space of the above mentioned model parameters.[24] Locating a number of real binary transition metals (CoPt, NiPt, CuAu) in these maps has elucidated their mixing behavior, which could not be explained by previous approaches including only diagonal disorder.[21,22]

IV. SURFACE SEGREGATION TRENDS

From the calculations with our model for the (001) and the (111) surface, we found very similar surface segregation trends. Therefore we will only present the results for the (001) surface, obtained from differences in the electronic energy for lattice slab configurations. Indeed, in most cases, the anisotropy of surface segregation is such that the phenomenon is weakened when going from open to close-packed surfaces, without reversing the nature of the segregating species. The only very few cases where such a reversal could be observed concerns systems for which the difference in surface energies is (very) small or vanishing while the size effect is strong. In these cases, surface relaxation becomes the main driving force behind surface segregation, giving rise to a larger orientation dependence. Examples are PtNi or PtCo systems.[4,14]

A direct way to determine the effective surface potential Δh^s is to calculate it from the energy difference between two slab configurations with equal composition x_B and equal number of nearest neighbors of type AB, N_{AB}, but with different occupations of the surface sites, that is with a different ΔN^s. In that case, it follows from Eq. (13) that

$$\Delta h^s = \frac{2(E_1 - E_2)}{\Delta N_1^s - \Delta N_2^s}, \tag{17}$$

where the subscripts 1 and 2 label the two slab configurations. Three examples of suitable slabs configurations for the composition $x_B = 0.5$ are drawn schematically in Figs. 3(a)–3(c). In each case, two mirror slab configurations can be obtained by swapping the chemical identity of the particles. The energy difference $E_1 - E_2$ between these two mirror configurations allows us to calculate Δh^s via Eq. (17).

In order to see to what extent the earlier mentioned correspondence between the effective surface potential and the difference in the pure component surface energies remains valid when off-diagonal disorder is taken into account, we have to compare Δh^s to $\Delta E^s = E_A^s - E_B^s$, calculated within the same tight-binding model, where the respective d-band fillings of the pure metals (A,B) have been taken equal to the partial d-band filings ($N_{e,A}$, $N_{e,B}$) in the alloy phases, consistently with DFT results.[46] These were determined in an approximate way as follows. First, for given total d-band

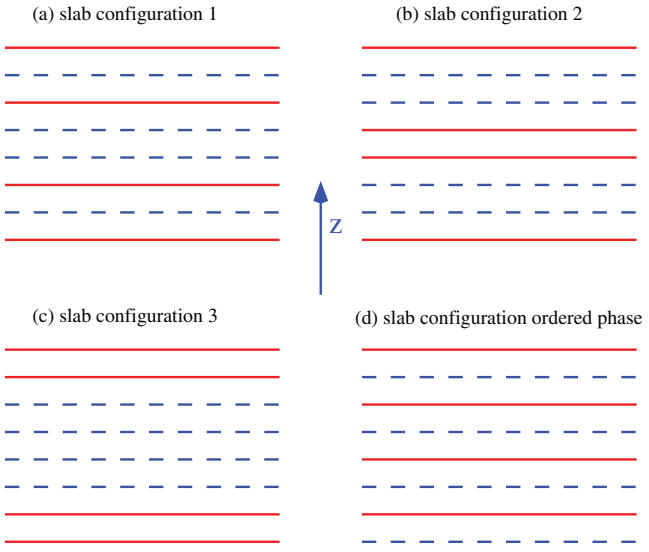

FIG. 3. (Color online) Schematic presentation of the slab configurations used for the calculation of the effective surface potential. Solid and dashed lines represent chemically different layers.

filling N_e we determine the Fermi level E_F for a system composed of the two pure bulk phase with a total density of states $n(E) = N_A n_A(E) + N_B n_B(E)$, thus without including an interphase contribution. Next, we determine the partial d-band fillings $N_{e,a}(a = A, B)$ according to

$$N_{e,a} = \int_{-\infty}^{E_F} n_a(E) dE. \tag{18}$$

After that we calculate the pure component surface energies $E_a^s(N_{e,a}) = E_i^{\text{slab}}(N_{e,a}) - E_a^{\text{bulk}}(N_{e,a})(a = A, B)$ for the calculated $N_{e,a}$ and, finally, $\Delta E^s(N_e)$ by

$$\Delta E^s(N_e) = E_A^s(N_{e,A}) - E_B^s(N_{e,B}). \tag{19}$$

In Fig. 4, we show the effective surface potential as a function of N_e for the slab configurations 1, 2, and 3 in Fig. 3 with composition $x_B = 0.5$ and different values of δ_d and δ_{nd}, calculated using the direct method [see Eq. (17)], and we compare it to ΔE^s [see Eq. (19)]. The agreement between Δh^s and ΔE^s is quite good in this equimolar case, also for nonzero nondiagonal disorder. Looking at the results for $\delta_d = 1$ and 4 eV and $\delta_{nd} = 0$ in the middle panels, we recover a result in agreement with the known, rough trend and previous calculations based on TBIM,[23] namely, a tendency for component A/B to segregate to the surface for low/high band filling, getting stronger with increasing δ_d (note the difference in scale on the vertical axis between left and right panels). Similar as for the effective pair interactions, the behavior of the effective surface potential can be qualitatively understood from the involved densities of states. The LDOS for a particle at the surface is narrower than that of a bulk particle, implying a transfer of the states at the band edges toward the center of the band. For a slab with component B at the surface, this gives a loss of states at the lower band edge with energies lower than those lost at the lower edge of the LDOS of component A at the surface, simply because B band is lower in energy due to its shift down (by δ_d) with respect to the A band. So the net loss of low-energy states is larger for a B terminated surface

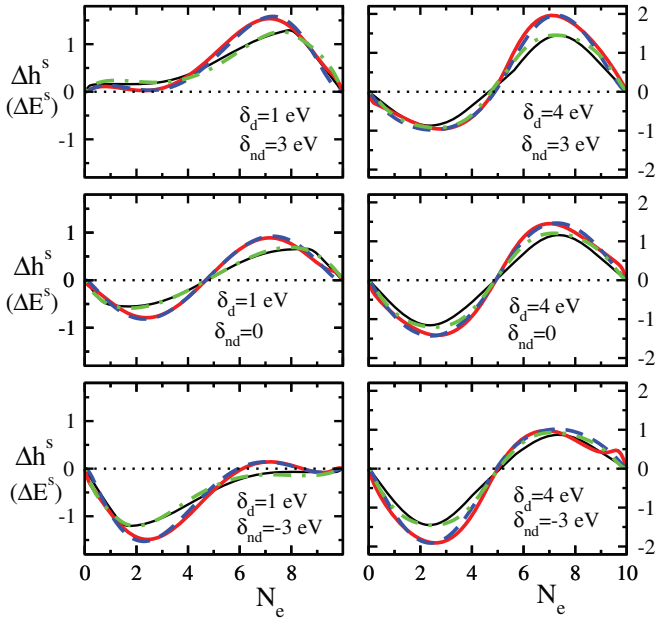

FIG. 4. (Color online) Calculated effective surface potential, Δh^s, for $L1_0$-like slabs with $x_B = 1/2$ based on the four slab configurations in Fig. 3 for $\delta_d = 1$ eV and different values of the off-diagonal parameter δ_{nd}, as indicated in the graphs. The solid (red), the dashed (blue), and the dashed-dotted (green) lines are the results using slab configurations 1, 2, and 3, respectively. The thin, solid (black) line represents the difference in the pure component surface energies ΔE^s, calculated using Eq. (19).

and this favors a surface terminated by the A component for low band filling ($N_e < 5$ eV).

If we now add off-diagonal disorder, we see a similar shift in the tendency as for the bulk mixing properties. Looking at the left top panel for $(\delta_d, \delta_{nd}) = (1,3)$ eV, the segregation tendency at low band filling of component A is strongly reduced or even reversed, while that of component B at high band filling is enhanced. Opposite behavior is seen for $(\delta_d, \delta_{nd}) = (1,-3)$ eV in the left bottom panel. The same shift in the trends occurs for the case $\delta_d = 4$ eV, but here the basic trend remains fully intact. Nevertheless, the extreme values of Δh^s change as much as 0.5 eV in these cases.

Comparing the results in Fig. 4, we notice that there is a systematic, relatively small difference connected with the occupancy of the subsurface layer, either by the same component that occupies the surface layer or not. This ambiguity in the calculated effective surface potential is to be attributed to the truncation/approximations of the cluster expansion leading to the TBIM. In the present case, this ambiguity could be (partly) resolved by assuming different values for the pair potentials involving surface atoms, which would give rise to additional parameters. However, the fact that the differences are relatively small confirms the rigorousness of the observed trends, without requiring further refinement.

We also studied the segregation trends for alloys with compositions different from $x_B = 0.5$, including the $L1_2$ ordered phase compositions $x_B = 0.25$ and 0.75 and diluted mixtures. In the $L1_2$ structure the conventional (cubic) unit cell of the fcc structure contains three A and one B atoms or vice versa. For such compositions, the procedure to compute

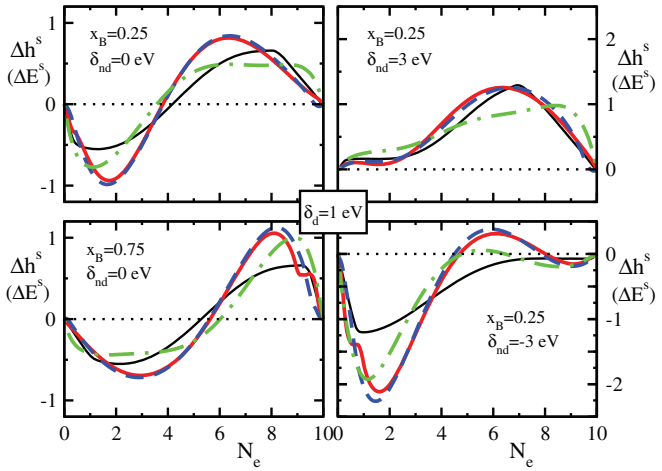

FIG. 5. (Color online) Calculated effective surface potential for three $L1_2$-like slabs based on the schematic pictures in Fig. 3 with the overall compositions $x_B = 1/4$ or $x_B = 3/4$, $\delta_d = 1$ eV, and different δ_{nd}, as indicated. The solid (red), dashed (blue) and dashed-dotted (green) line are the results using two realizations of the slab 1, 2, and 3, respectively, combined with the slab in Fig. 3(d) (see text). The thin, solid (black) lines represent ΔE^s.

the effective surface potential from the energy difference of mixed slabs is slightly more complicated. Note that taking the chemical image of a slab with composition $x_B \neq 0.5$ still conserves N_{AB} but not the composition that transforms into $1 - x_B$, making Eq. (17) inapplicable. To overcome this difficulty for the $L1_2$ compositions, we computed the effective surface potential from the energies of three slabs with different N_{AB} and ΔN^s by solving a set of three linear equations (13) for for $C(=\sum_a N_a E_a + \frac{1}{2} N^s \Sigma^s)$, V, and Δh^s. Three such slabs were selected by using again the schematic picture in Fig. 3, but now with the solid and dashed lines representing pure layers and layers with composition 0.5, respectively, like in the $L1_2$ phase with an overall composition either $x_B = 0.25$ or 0.75. For each of the slab configurations 1, 2, and 3 in Fig. 3, a second slab with equal x_B but different N_{AB} and ΔN^s is obtained by replacing each pure by a mixed layer and each mixed by a pure layer. To complete the set, the third slab configuration is taken to be the one in Fig. 3(d) with again equal composition but different N_{AB} and ΔN^s.

The results, including a comparison with ΔE^s, are shown in Fig. 5 for different model parameters. From the results in the left panels for the two $L1_2$ compositions and $(\delta_d, \delta_{nd}) = (1,0)$ eV, the first important things to notice are that (i) globally the shape of the curve is the same as those for the composition $x_B = 0.5$ in Fig. 4 and (ii) an asymmetry has occurred in the position where the curve crosses the zero line. The band fillings beyond which B terminated surfaces are favored have changed from $N_e = 5$ for $x_B = 0.5$ (see Fig. 4) to $N_e = 4$ for $x_B = 0.25$ and to $N_e = 5.8$ for $x_B = 0.75$. A comparable rather strong effect of the composition was also seen in extensive calculations of the effective pair interactions.[24] Next, if we add off-diagonal disorder, the effect is basically the same as that in Fig. 4, as is illustrated in the right panels for $x_B = 0.25$. It strongly favors the segregation of A/B to the surface for negative/positive δ_{nd}.

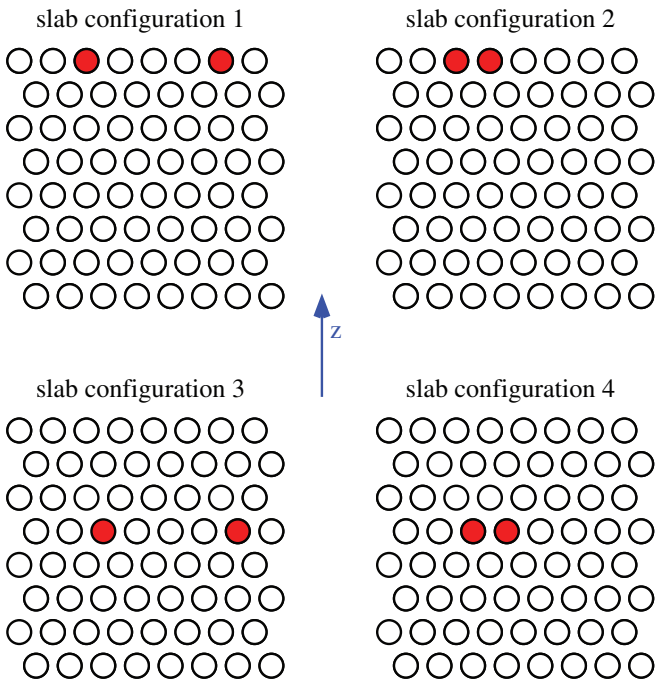

FIG. 6. (Color online) Schematic presentation of the slab configurations used for the calculation of the effective pair interactions and surface potential for diluted mixtures. The impurities in slabs 2 and 4 are first neighbors, contrary to the situation in slabs 1 and 3.

Although the different curves in Fig. 5, obtained for the different reference systems as explained, are still rather close, the variation is larger than in Fig. 4, and, in particular, the curve representing ΔE^s starts to deviate considerably, although the global trends remain the same.

To determine the effective surface potential for dilute mixtures we used the four slab configurations displayed schematically in Fig. 6, each of them with 2 impurities B sitting either in the bulk or at the surface of an A lattice, and being neighbors or not. Using Eq. (13), the effective pair interactions can readily be obtained either from the energy difference between slab 1 and 2 or else from the energy difference between slab 3 and 4. As before, within the TBIM approximation, the two results, hereafter denoted as V_{1-2} and V_{3-4}, respectively, will not exactly be the same in general. However, the comparisons between the two results in the left panels of Fig. 7 for $\delta_d = 2$ eV and $\delta_{nd} = 0, -2$, and 2 eV again confirm the validity of the TBIM when it comes to retrieving the trends, as the results are in fact quite close. As for the nondiluted mixtures, there is a global trend to demix for low and high band filling and to mix for band fillings in between. However, the intersections with the $V = 0$ axis are extremely shifted to the left, so that the domain of demixing at low band filling has become very narrow. Moreover, in particular for $\delta_{nd} = -2$ eV, a new domain of mixing has appeared at high band filling. (We did similar calculations for mixtures diluted in A. In that case, the intersections with the $V = 0$ are shifted completely to the right.)

Once the effective pair interaction is determined, we can calculate the effective surface potential either from the energy difference between slab 1 and 3 or from the energy difference between slab 2 and 4 by using again Eq. (13) and eliminating

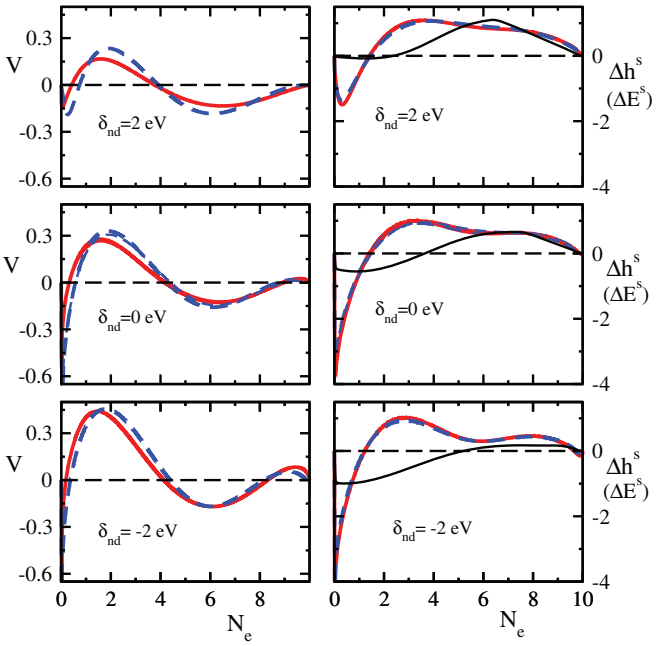

FIG. 7. (Color online) Calculated effective pair interactions (left panels) and surface potential (right panels) for a diluted mixture, made of two impurities B in a A bulk, $\delta_d = 2$ eV and different values for the off-diagonal parameter, as indicated. The solid (red) and dashed (blue) lines in the left panels are V_{1-2} and V_{3-4}, while those in the right panels represent Δh^s_{1-3} and Δh^s_{2-4}, respectively (see text). The thin, solid (black) lines represent ΔE^s. Both middle panels contain the results for the cases in which the two impurities in slab 1 and 3 of Fig. 6 are taken as second, third, fourth, and fifth neighbors. All these results are so close that they can hardly be distinguished in the figure. For the calculations shown in the other panels, the impurities in slabs 1 and 3 were taken as fifth neighbors.

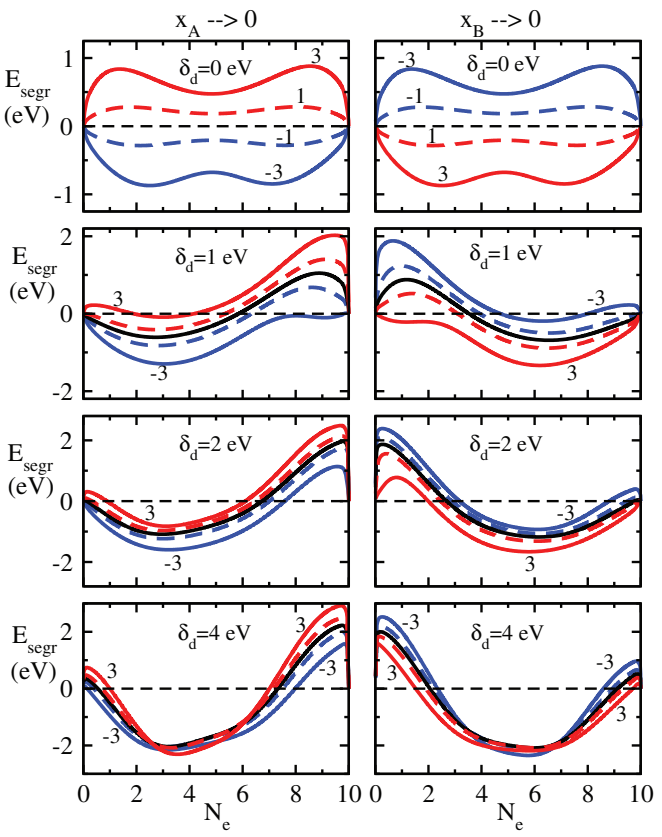

FIG. 8. (Color online) Electronic contribution to the segregation energy in both dilute limits for different values of diagonal and off-diagonal disorder parameters. Red, dashed red, black, dashed blue, and blue lines refer to $\delta_{nd} = 3$, 1, 0, -1, and -3 eV. Note the difference in the energy scale for graphs in different rows.

V by using V_{1-2} or V_{3-4}, or else $V = (V_{1-2} + V_{3-4})/2$ as we did. The respective results, which we will denote as Δh^s_{1-3} and Δh^s_{2-4} are shown in the right panels of Fig. 7 and compared to ΔE^s from Eq. (19). The global trends, including the effect of off-diagonal disorder, are the same as for the nondilute mixtures, but the range of band fillings yielding negative Δh^s has become much smaller now. In practice, this means that there is an enhanced tendency for the B solute to segregate to the surface. However, while the results for Δh^s_{1-3} and Δh^s_{2-4} are quite close, they deviate considerably from ΔE^s, in particular, for low band filling, where it predicts an opposite surface segregation trend over a significant range of N_e. It is worth noticing that Δh^s_{1-3} and Δh^s_{2-4} are much more reliable indicators for the segregation trend than ΔE^s, as the former quantities are directly obtained from the diluted mixtures. This leads us to the conclusion that the rule of thumb to predict the surface segregation trend from the difference in surface energy of the pure components can become very inaccurate for diluted mixtures.

This is confirmed by calculating directly the segregation energy, $E_{\rm segr}$, of an impurity in the framework of the same FMA model. We calculate $E_{\rm segr}$ standardly as the energy of a slab with a single impurity at the surface minus that of a slab with an impurity in the bulk part of the slab. As can be seen in Fig. 8, the overall behavior is dominated by the diagonal term as soon as it is sufficiently large ($\delta_d \geqslant 2$), but it is strongly modified by the off-diagonal disorder effect otherwise ($\delta_d < 2$). Moreover, the importance of this effect is stronger at low or high band filling. Within the TBIM approximation, $E_{\rm segr} = (-)\Delta h^s + 4V$ when the impurity is $A(B)$, implying that $E_{\rm segr}$ includes both the energetic contribution from the surface term and that of the alloying term. Comparing then the right column of Fig. 8 to that of Fig. 7 we can deduce that, when Δh^s differs from the difference in surface energies between pure elements, it is the difference in effective surface potentials (Δh^s) [together with the contribution from the alloying term ($4V$)] that drives surface segregation.

V. CONCLUSIONS

We have revisited the problem of surface segregation in binary tansition metal alloys on the basis of a d-band tight-binding model within the fourth moment approximation (FMA), which includes both diagonal disorder δ_d, that is, the energy shift between the d bands of the two components, and off-diagonal disorder δ_{nd}, which takes into account the difference in the pure component bandwidths. By including both effects simultaneously, the present study goes beyond previous studies,[23] and reveals strong systematic trends in the surface segregation properties as a function of the band filling N_e, δ_d, and δ_{nd}, and also of the composition x_B of

the mixture. While for $\delta_{nd} = 0$ old results are recovered, predicting A/B terminated surfaces for a less/more than a half-filled d band (i.e., $N_e = 5$), the effect of a nonzero δ_{nd} is to strongly asymetrize and even reverse this tendency favoring the segregation of A/B for negative/positive δ_{nd}.

In addition, the present study shows the limits of the usual argument based on the difference in surface energies to predict surface segregation in the dilute limits. From a more general point of view, the present work extends a previous work[24] on bulk mixing trends to surface segregation trends. Our approach, or more generally a tight-binding approach, is particularly appropriate for unravelling the trends in the mixing and surface segregation properties, as it allows for the identification of a very limited set of model parameters, which cover the whole transition metal family and which turn out to be the main driving forces behind the trends.

A further interest of using the FMA model lies in the fact that this model allows for large scale, atomistic simulations with a computation time that scales linearly with the system size and is not much slower than the currently widely used models based on the SMA approximation. At the same time, FMA remains close to standard tight binding and is therefore expected to be more reliable and transferable than SMA. This is indeed confirmed by the roughly correct prediction of the trends in the bulk ordering and segregation properties of transition metal alloys, as found in this work. In addition, since FMA provides an approximation of the electronic structure, completely absent in standard SMA models, it opens the possibility to do large scale simulations designed for retrieving dynamical properties involving the electronic structure.

ACKNOWLEDGMENTS

This work was founded by the French National Agency ANR through SimNanA Project No. ANR-08-NANO-003. We thank all the partners of this consortium for enlightening discussions. We also acknowledge support from the COST Action MP0903.

[1] J. D. Rittner, S. M. Foiles, and D. N. Seidman, Phys. Rev. B **50**, 12004 (1994).
[2] P. Wynblatt and A. Landa, Comput. Mater. Sci. **15**, 250 (1999).
[3] A. V. Ruban and H. L. Skriver, Comput. Mater. Sci. **15**, 119 (1999).
[4] G. Tréglia, B. Legrand, F. Ducastelle, A. Saúl, C. Gallis, I. Meunier, C. Mottet, and A. Senhaji, Comput. Mater. Sci. **15**, 196 (1999).
[5] A. Christensen, A. V. Ruban, P. Stoltze, K. W. Jacobsen, H. L. Skriver, J. K. Norskov, and F. Besenbacher, Phys. Rev. B **56**, 5822 (1997).
[6] A. V. Ruban, H. L. Skriver, and J. K. Norskov, Phys. Rev. B **59**, 15990 (1999).
[7] M. Polak and L. Rubinovich, Surf. Sci. Rep. **38**, 127 (2000).
[8] P. M. Ossi, Surf. Sci. **201**, L519 (1988).
[9] Y. Gauthier and R. Baudoing, in *Surface Segregation Phenomena*, edited by P. A. Dowben and A. Miller (CRC Press, Florida, 1990), p. 169.
[10] *The Chemical Physics of Solid Surface*, edited by D. P. Woodruff, Surface Alloys, and Alloy Surfaces Vol. 10 (Elsevier Science B.V., Amsterdam, The Netherlands, 2002).
[11] J. H. Sinfelt, *Bimetallic Catalysts: Discoveries Concepts and Applications* (Wiley, New York, 1983).
[12] R. L. Johnston and R. Ferrando in *Faraday Discussion 138*: *Nanoalloys: From Theory to Application*, *Birmingham, 2007* (RSC Publishing, United Kingdom, 2008).
[13] D. Alloyeau, C. Mottet, and C. Ricolleau, *Nanoalloys, Synthesis, Structure and Properties*, Engineering Materials (Springer-Verlag, London, 2012).
[14] J.-M. Roussel, G. Tréglia, and B. Legrand, Solid State Phenomena **172–174**, 1008 (2011).
[15] P. Wynblatt and R. C. Ku, in *Interfacial Segregation*, edited by W. C. Johnson and J. M. Blakely (AMS, Metals Park, OH, 1979), p. 115.
[16] J. Creuze, I. Braems, F. Berthier, C. Mottet, G. Tréglia, and B. Legrand, Phys. Rev. B **78**, 075413 (2008).
[17] G. H. Jóhannesson, T. Bligaard, A. V. Ruban, H. L. Skriver, K. W. Jacobsen, and J. K. Norskov, Phys. Rev. Lett. **88**, 255506 (2002).
[18] L. Delfour, J. Creuze, and B. Legrand, Phys. Rev. Lett. **103**, 205701 (2009).
[19] F. Calvo and C. Mottet, Phys. Rev. B **84**, 035409 (2011).
[20] F. Ducastelle, *Order and Phase Stability in Alloys*, Vol. 3 (North-Holland/Elsevier Science Publishers, Amsterdam, 1991).
[21] F. Ducastelle and F. Gautier, J. Phys. F: Met. Phys. **6**, 2039 (1976).
[22] A. Bieber, F. Ducastelle, F. Gautier, G. Tréglia, and P. Turchi, Solid State Commun. **45**, 585 (1983).
[23] G. Tréglia, B. Legrand, and F. Ducastelle, Europhys. Lett. **7**, 575 (1988).
[24] J. H. Los, C. Mottet, G. Tréglia, and C. Goyhenex, Phys. Rev. B **84**, 180202(R) (2011).
[25] M. W. Finnis and J. E. Sinclair, Philos. Mag. A **50**, 45 (1984).
[26] V. Rosato, M. Guillopé, and B. Legrand, Philos. Mag. A **59**, 321 (1989).
[27] S. Karoui, H. Amara, B. Legrand, and F. Ducastelle, J. Phys.: Condens. Matter **25**, 056005 (2013).
[28] S. M. Foiles, M. I. Baskes, and M. S. Daw, Phys. Rev. B **33**, 7983 (1986).
[29] M. I. Baskes, Phys. Rev. Lett. **59**, 2666 (1987).
[30] M. I. Baskes, J. S. Nelson, and A. F. Wright, Phys. Rev. B **40**, 6085 (1989).
[31] F. Cleri and V. Rosato, Phys. Rev. B **48**, 22 (1993)
[32] J. Cai and J. S. Wang, Phys Rev. B **64**, 035402 (2001).
[33] J. Tersoff, Phys. Rev. Lett. **56**, 632 (1986).
[34] D. W. Brenner, O. A. Shenderova, J. A. Harrison, S. J. Stuart, B. Ni, and S. B. Sinnott, J. Phys.: Condens. Matter **14**, 783 (2002).
[35] A. C. T. van Duin, A. Strachan, S. Stewman, Q. Zhang, X. Xu, and W. A. Goddard, III, J. Phys. Chem. A **107**, 3803 (2003).
[36] J. H. Los, L. M. Ghiringhelli, E. J. Meijer, and A. Fasolino, Phys. Rev. B **72**, 214102 (2005).
[37] H. Amara, J. M. Roussel, C. Bichara, J. P. Gaspard, and F. Ducastelle, Phys. Rev. B **79**, 014109 (2009).
[38] J. H. Los, C. Bichara, and R. J. M. Pellenq, Phys. Rev. B **84**, 085455 (2011).
[39] D. G. Pettifor, Phys. Rev. Lett. **63**, 2480 (1989).
[40] I. I. Oleinik and D. G. Pettifor, Phys Rev. B **59**, 8500 (1999).

[41]D. G. Pettifor and I. I. Oleinik, Phys. Rev. Lett. **84**, 4124 (2000).
[42]V. Kuhlmann and K. Scheerschmidt, Phys. Rev. B **76**, 014306 (2007)
[43]A. Saùl and M. Weissmann, Phys. Rev. B **60**, 4982 (1999).
[44]D. A. Papaconstantopoulos, *Handbook of Electronic Structure of Elemental Solids* (Plenum, New York, 1986).
[45]J. C. Slater and G. F. Koster, Phys. Rev. **94**, 1498 (1954).
[46]A. Jaafar, C. Goyhenex, and G. Tréglia, J. Phys.: Condens. Matter **22**, 505503 (2010).
[47]R. Haydock, in *Solid State Physics*, edited by F. Seitz, D. Turnbull, and H. Ehrenreich (Academic, New York, 1980), Vol. 35.
[48]G. Allan, M. C. Desjonquéres, and D. Spanjaard, Solid State Commun. **50**, 401 (1984).
[49]C. Goyhenex and G. Tréglia, Phys. Rev. B **83**, 075101 (2011).